JOURNAL OF THE ROYAL SOCIETY Interface

# Can a fibrillar interface be stronger and tougher than a non-fibrillar one?

Tian Tang, Chung-Yuen Hui and Nicholas J Glassmaker

*J. R. Soc. Interface* 2005 **2**, 505-516
doi: 10.1098/rsif.2005.0070

JOURNAL OF THE ROYAL SOCIETY Interface

*J. R. Soc. Interface* (2005) **2**, 505–516
doi:10.1098/rsif.2005.0070
*Published online* 12 August 2005

# Can a fibrillar interface be stronger and tougher than a non-fibrillar one?

**Tian Tang[1,†], Chung-Yuen Hui[1] and Nicholas J. Glassmaker[2]**

[1]*Department of Theoretical and Applied Mechanics, Cornell University, Ithaca, NY 14853, USA*
[2]*Department of Chemical Engineering, Lehigh University, Bethlehem, PA 18015, USA*

Elasticity analysis and finite element simulations are carried out to study the strength of an elastic fibrillar interface. The fibrils are assumed to be in perfect contact with a rigid substrate. The adhesive interaction between the fibrils and the substrate is modelled by the Dugdale–Barenblatt model (DB). The condition for a fibrillar interface to be stronger than a non-fibrillar one is obtained for two regimes: (i) small fibril or flaw insensitive regime; (ii) large fibril or flaw sensitive regime. The transition between the two regimes is characterized by a dimensionless parameter that incorporates the material constants of the elastic fibrils and interfacial properties. The condition for a fibrillar interface to be tougher is also given. Lateral collapse is found to be detrimental to the strength and toughness of a fibrillar interface.

**Keywords: adhesion; fibrillar interface; strength; toughness; pull-off stress**

## 1. INTRODUCTION

It is widely accepted that the quality of adhesion between an adhesive and a hard substrate depends on surface interactions as well as the viscoelastic behaviour of the adhesive. Viscoelasticity is one of the main reasons why most adhesives are not reversible since it causes energy dissipation, which leads to adhesion hysteresis. Elastic materials such as polydimethylsiloxane (PDMS) typically have very low work of adhesion since the surface interaction forces are of van der Waals type. In comparison with interfaces reinforced by hydrogen or covalent bonding, the strength of interfaces supported by van der Waals interaction is low. Hence, it is a considerable challenge to develop an adhesive that possesses high strength, a large practical work of adhesion and a recoverable microstructure. However, the potential for such adhesives is evident from recent studies of adhesion in geckos and other animals (Rischick *et al.* 1996; Autumn *et al.* 2000; Scherge & Gorb 2001). Specifically, the feet of most geckos contain highly fibrillated substructures that give them the ability to adhere to and separate from a wide variety of surfaces by relying only on weak dispersive forces. Despite the low intrinsic energy required to separate surfaces held together by these forces, these organisms achieve remarkably strong, reversible adhesion, which is evident by their ability to rapidly climb up smooth vertical surfaces.

There have been several efforts (Campolo *et al.* 2003; Geim *et al.* 2003; Sitti & Fearing 2003; Glassmaker *et al.* 2004; Hui *et al.* 2004; Peressadko & Gorb 2004) to fabricate model fibrillar structures with very small fibrils (less than 5 μm in diameter) in order to replicate the dimensions of fibrils found on geckos. These experiments show that fibrillar samples exhibit larger pull-off stress per unit *actual* contact area than non-fibrillar smooth controls. However, the force required to pull-off a unit area of fibrillar interface is still less than non-fibrillar smooth controls[1] due to a large decrease in total contact area in the fibrillar samples. This indicates that the loss of contact area still outweighs the increase in adhesion due to small fibrils. A plausible explanation is that it is extremely difficult for a large number of small fibrils to maintain uniform contact, as pointed out by Glassmaker *et al.* (2004). Surface roughness can also significantly reduce the effective work of adhesion between the attachment and the substrate (Persson & Tosatti 2001; Persson & Gorb 2003; Hui *et al.* in press). Buckling of fibrils has also been shown to be detrimental to adhesion (Hui *et al.* in press).

The following question naturally arises: is it possible for an elastic fibrillar interface to be stronger and tougher than a non-fibrillar one of the same materials, assuming that the surfaces are in perfect uniform contact?

In this work, the terms strength and toughness are used in the following sense. The strength $F_s$ of the fibrillar/non-fibrillar interfaces shown in figure 1*a*,*b* is defined as the applied load needed to fail the entire

[†]Author for correspondence (tt88@cornell.edu).

[1]The experiments by Geim *et al.* (2003) showed that the actual force to pull-off a fibrillar structure is higher than the non-fibrillar smooth control. Using a very similar system, we have been unable to repeat their experimental results (Hui *et al.* 2004). Specifically, we found that the overall adhesion is reduced for the same fibrillar structure.

*Received* 13 May 2005
*Accepted* 23 July 2005

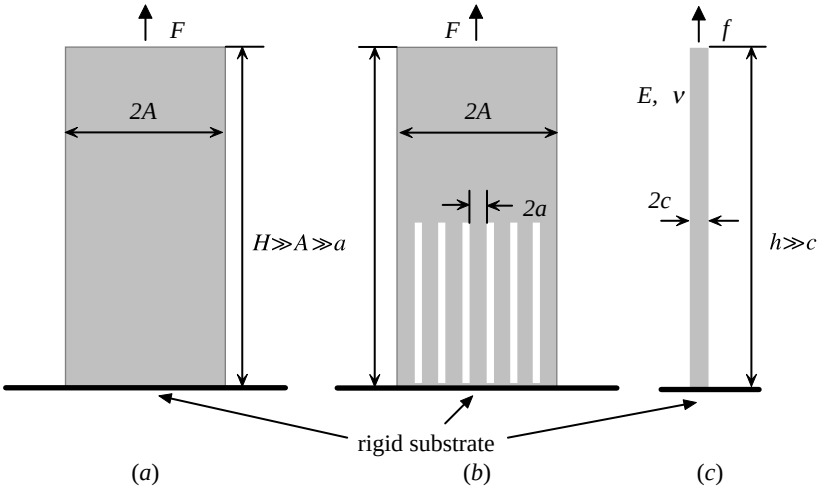


Figure 1. (*a*) Non-fibrillar structure: force $F$ on an elastic cylindrical flat punch with radius $A$. (*b*) Fibrillar structure: force $F$ on many identical small elastic cylindrical fibrils with radius $a \ll A$. (*c*) Force $f$ on a single elastic fibre with radius $c$, Young's modulus $E$ and Poisson's ratio $\nu$. In all the three structures, the height of the fibres is assumed to be much larger than other dimensions.

interface; whereas the energy $W_f$ expended during this process is defined as the toughness. Thus, the strength and toughness of a structure will in general depend on geometric factors such as sample size and fibril diameter. While there is no conclusive evidence to indicate that the strength of man-made fibrillar interface is greater than that of a smooth non-fibrillar one, recent experiments (Hui *et al.* 2004) on a model system showed that a fibrillar structure that is well bonded to a substrate is tougher than a non-fibrillar one.[2] Unfortunately, their experimental set-up did not allow them to probe the question of strength.

Since in many applications strength is more important than toughness, we first address the following question: is it theoretically possible for the fibrillar structure in figure 1*b* to have a higher strength than the non-fibrillar structure in figure 1*a*? If so, what is the relationship between strength and geometry? In addition, is it possible to have both high strength and toughness in a purely elastic system?

In the following, we assume that the structures in figure 1*a*,*b* are in perfect uniform contact with a smooth rigid substrate. Specifically, in figure 1*a*, a cylindrical flat end punch or a very large fibre, of radius $A$, is in contact with a rigid substrate. In figure 1*b*, many identical small cylindrical fibrils, of radius $a \ll A$, are bonded to the same punch end and are attached to the same rigid substrate. The height of these fibrils is assumed to be much greater than their diameter so that at distances far from the contact, each fibril is subjected to the same uniaxial tension $\sigma = F/(\omega\pi A^2)$, where $F$ is the applied load and $\omega$ is the area fraction occupied by the fibrils. At first glance, it may seem that the smooth non-fibrillated punch in figure 1*a* will have higher strength, since it has more contact area. This is not a foregone conclusion since the edge of the punch as well as the edge of a typical fibril is a stress concentrator. We will show that it is possible for the unfibrillated structure in figure 1*a* to fail at a lower strength even though the fibrils in figure 1*b* may be subjected to a higher tensile stress. Of course, this scenario is possible only if the strength of the fibrils increases as fibril radius decreases. To make this concept precise, let $f_s(c)$ be the strength of a fibre of radius $c$ as shown in figure 1*c*. Denote the average tensile stress to fail this fibre by $\sigma_s(c)$, i.e.

$$\sigma_s(c) = f_s(c)/\pi c^2. \tag{1.1}$$

The force required to fail the unfibrillated structure in figure 1*a*, i.e. its strength $F_s(A)$, is obtained by setting $c = A$ in (1.1), i.e.

$$F_s(A) = f_s(A) = \pi A^2 \sigma_s(A). \tag{1.2}$$

Similarly, the fibrillar structure in figure 1*b* fails when the applied force reaches

$$F_s(a) = N f_s(a) = \omega\pi A^2 \sigma_s(a), \tag{1.3}$$

where $N$ is the total number of fibrils, and $\omega = Na^2/A^2$ is the area fraction of the fibrils. Now, the strength of the fibrillar structure is higher than the unfibrillar one if and only if

$$F_s(a) > F_s(A). \tag{1.4}$$

Using equations (1.2) and (1.3), (1.4) can be rewritten as

$$\omega\sigma_s(a) > \sigma_s(A). \tag{1.5}$$

Thus, we have reduced the problem of comparing strength to finding the stress $\sigma_s(c)$ required to detach a cylindrical elastic fibre of arbitrary radius $c$ from a rigid substrate. It should be noted that, for simplicity, we have denoted the pull-off stress $\sigma_s$ by $\sigma_s(c)$, indicating its dependence on the fibre radius $c$. Of course, $\sigma_s$ also depends on the elastic constants of the fibre, as well as interfacial adhesion. Later, we show that when properly normalized, $\sigma_s$ depends on a single dimensionless parameter $\chi$ which is a function of these quantities.

The plan of this paper is as follows. In §2, we introduce the cohesive zone model used to characterize

[2]Uniform contact was achieved by bonding the fibrils which are macroscopic in size to a glass substrate.

the adhesion on the fibre/substrate interface. In §3, we determine the single fibre pull-off stress $\sigma_s$ using asymptotic analysis and finite element simulations. In §4, we give the conditions for a fibrillar interface in figure 1*b* to have higher strength than a non-fibrillar interface in figure 1*a*. The question of toughness is addressed in §5. Discussions and conclusion are given in §6.

## 2. MODEL FOR INTERFACE FAILURE

To determine the single fibre pull-off stress $\sigma_s$, we need to model the interfacial adhesion, that is, the attractive forces between adhering surfaces. Since molecular interactions between macroscopic bodies are usually negligible except near surfaces, we assume that adhesive interactions occur as surface tractions $\boldsymbol{T}$, which depend only on the separation $\boldsymbol{\delta}$ between the surfaces. Such models, i.e. so called cohesive zone models, have been employed to study interfacial failure in a large number of material systems (Dugdale 1960; Barenblatt 1962; Rose *et al.* 1981; Xu & Needleman 1994). It turns out that the condition for interfacial failure is insensitive to the functional form of the cohesive zone model, provided that the cohesive strength and the work of adhesion of the two models are the same (Maugis 1992).

For interfaces which fail in tension, a simple model is the DB model (Dugdale 1960; Barenblatt 1962). In this model, the interface is allowed to separate from the substrate when the normal traction $\sigma$ on the interface reaches a tensile value $\sigma_0$. The interface fails or can no longer support traction when the normal separation $\delta > \delta_c$. For obvious reasons, $\sigma_0$ is called the intrinsic strength of the interface, which together with $\delta_c$, are material constants. In the DB model, the work of adhesion $W_{ad}$ of the surfaces in contact is the area under the $\sigma$–$\delta$ plot shown in figure 2, i.e. $W_{ad} = \sigma_0\delta_c$.

In addition to the normal attractive forces, the interface is also subjected to shear stresses, due to Poisson contraction. In the following, we assume friction is sufficiently high so that no slip is allowed along the interface. This is a very good approximation for a soft material contacting a rigid surface. With this assumption, the interface can only fail in the normal direction.

## 3. DETERMINATION OF SINGLE FIBRE PULL-OFF STRESS $\sigma_s$

The geometry is illustrated in figure 1*c*. A load $f$ is applied to a long elastic fibre of radius $c$. The fibre is assumed to be linearly elastic with Young's modulus $E$ and Poisson's ratio $\nu$. Because the fibre is long in comparison with $c$, the stress in the fibre far way from the interface is in pure tension and is given by $\sigma = f/\pi c^2$. Our goal is to determine the pull-off force $f_s$ or equivalently, the pull-off stress $\sigma_s = f_s/\pi c^2$.

To motivate the analysis, we note that if the intrinsic strength $\sigma_0$ could be infinite, the stresses at the fibre edge would also be infinite, since, as will be shown below, the stresses at the fibre edge are singular in the elasticity solution. The fact that the intrinsic strength

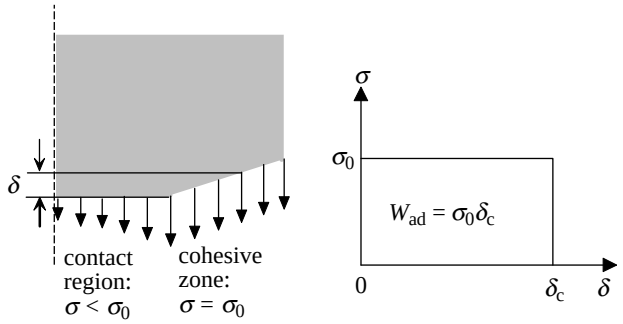


Figure 2. Dugdale–Barenblatt (DB) model. Work of adhesion $W_{ad} = \sigma_0\delta_c$; $\sigma_0$ is the interfacial strength and $\delta_c$ is the opening displacement at failure.

is finite implies that the singular stresses predicted by the elastic solution cannot be valid near the edge. Indeed, according to the DB model, the interface will separate (i.e. $\delta > 0$) at a critical stress of $\sigma_0$. The region of the interface where separation occurs is called the cohesive zone. The DB model states that the normal stress in the cohesive zone is constant and equal to the intrinsic strength $\sigma_0$. Physically, one anticipates that the maximum interfacial separation occurs at the fibre edge. This maximum interfacial separation $\delta_{max}$ depends on the applied load $f$. When $f$ reaches a critical value $f_s$, $\delta_{max}$ reaches $\delta_c$. At this point the interface near the edge can no longer support normal stress, and crack initiation starts. Because the fibre is long in comparison with its radius, crack growth occurs under load control, which is anticipated to be unstable. Therefore, we expect that pull-off will occur once a crack is initiated. This result was confirmed by our finite element simulations.

The dependence of the pull-off stress on the fibre size is a consequence of the fact that the region of dominance of the elastic singular stress field scales with $c$. Specifically, if $c \gg l_c$, where $l_c$ denotes the length of the cohesive zone, there will be a region outside the cohesive zone where the elastic singular stress field still dominates. In this region, the normal stress on the interface is much smaller than $\sigma_0$; hence the average stress on the fibre can be much smaller than $\sigma_0$ when the crack initiates. On the other hand, if $c \approx l_c$, the elastic singular stress field has no region of dominance. In this case, the cohesive zone occupies the entire fibre/substrate interface; the average pull-off stress reaches its theoretical limit, i.e. $\sigma_s = \sigma_0$. Therefore, large $c$ favours the concentration of stress near the fibre edge, resulting in pull-off at low applied force.

We attack the problem of determining $\sigma_s$ in two ways: firstly, we establish a scaling law based on asymptotic analysis. Secondly, we compute $\sigma_s$ using finite element method. The scaling law will be used to interpret the result of our finite element simulations.

### 3.1. Asymptotic analysis

In the limit of infinite interfacial strength, the stresses at the fibre edge are infinite. The exact form of the stresses in this case can be obtained using an asymptotic analysis method based on classical work in

elasticity (Bogy & Wang 1971; Dempsey & Sinclair 1981). Details that are relevant to our specific problem are given in appendix A. Here we state the relevant results.

Let $(x, y, z)$ be a local Cartesian coordinate system at the fibre edge, as shown in figure 3*a*. For an elastic fibre on a rigid substrate, the normal stress $\sigma_{zz}$ near the fibre edge has the form

$$\sigma_{zz}(x \to 0, y = z = 0) = Cx^{-\lambda}, \tag{3.1}$$

where $0<\lambda<1$ is a numerical factor which depends on the Poisson's ratio, e.g. $\lambda \cong 0.4$ for $\nu = 0.5$. Values of $\lambda$ for other $\nu$ are given in appendix A. In (3.1), $C$ is a constant which depends on the loading conditions and cannot be determined by asymptotic analysis. Linear elasticity and dimensional considerations imply that

$$C = \alpha\sigma c^{\lambda}, \tag{3.2}$$

where $\sigma \equiv f/\pi c^2$ is the average stress on the fibre and $\alpha$ is an unknown numerical factor of order one.

Equation (3.1) allows us to estimate the critical stress for pull-off, $\sigma_s$, in the limit where the cohesive zone is very small in comparison with the fibre radius. We call this limit the flaw sensitive regime. The length of the cohesive zone $l_c$ can be estimated by evaluating the stress given by (3.1) at $x = l_c$ and equating the result to the intrinsic strength $\sigma_0$. The cohesive length is found to be

$$l_c/c = (\alpha\sigma/\sigma_0)^{1/\lambda}. \tag{3.3}$$

From dimensional considerations, the maximum separation in the cohesive zone, $\delta_{max} \equiv \delta(x = y = z = 0)$, has the form

$$\delta_{max} = q\frac{\sigma_0}{E^*} l_c, \tag{3.4}$$

where $E^* \equiv E/(1-\nu^2)$, and $q$ is an unknown numerical factor of order 1. Substituting equation (3.3) into (3.4) gives

$$\delta_{max} = q\frac{c\sigma_0}{E^*}\left(\frac{\alpha\sigma}{\sigma_0}\right)^{1/\lambda}. \tag{3.5}$$

Applying the condition of pull-off, $\delta_{max} = \delta_c$, to equation (3.5) results in

$$\sigma_s = \sigma_0 B\chi^{-\lambda}, \tag{3.6}$$

where $B \equiv \alpha^{-1}(2\pi q)^{-\lambda}$ and $\chi$ is a dimensionless parameter defined by

$$\chi \equiv \sigma_0 c/2\pi E^* \delta_c = \sigma_0^2 c/2\pi E^* W_{ad}. \tag{3.7}$$

For equation (3.6) to be valid, the length of the cohesive zone must be much smaller than the fibre radius, i.e. $l_c/c \ll 1$. Using equations (3.3) and (3.6), this condition translates to $\chi \gg 1$, where we have neglected a numerical factor of order 1. The condition $\chi \gg 1$ corresponds to high interfacial strength, low fibre stiffness, or large fibre radius.

In the other limit, which we shall refer to as the flaw insensitive regime, $\chi \ll 1$, corresponding to low intrinsic strength, high fibre stiffness, or small fibre radius. In this regime, the cohesive zone occupies the entire interface; and the pull-off stress is simply

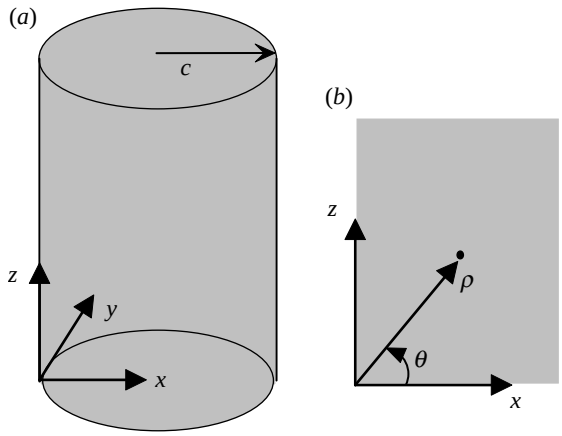


Figure 3. (*a*) Local Cartesian coordinates at the corner of a cylindrical flat end fibre. (*b*) Local polar coordinates at the corner of the fibre.

$$\sigma_s = \sigma_0. \tag{3.8}$$

That is, while equation (3.6) predicts $\sigma_s/\sigma_0 \to \infty$ as $\chi \to 0$, the pull-off stress is actually limited by the cohesive strength.

The above analysis suggests that, for a given Poisson's ratio, the normalized pull-off stress $\sigma_s/\sigma_0$ depends only on a single dimensionless parameter $\chi$, i.e.

$$\sigma_s/\sigma_0 = \Phi(\chi), \tag{3.9}$$

where $\Phi(\chi)$ is a dimensionless function which has the property

$$\Phi(\chi) = \begin{cases} B\chi^{-\lambda} & \chi \gg 1, \\ 1 & \chi \ll 1. \end{cases} \tag{3.10}$$

The fact that for a given Poisson's ratio, the normalized pull-off stress $\sigma_s/\sigma_0$ depends only on $\chi$ can be proved rigorously. The proof of this result is given in appendix B. This result is relevant since it expedites the numerical analysis, as the effects of geometry, modulus, interfacial strength and work of adhesion are incorporated into a single parameter. This parameter $\chi$ has also been mentioned by Gao *et al.* (2005) in their work to study the pull-off of a single fibre from a rigid substrate with a pre-existing edge crack (a defect). Unlike the crack initiation problem we study here, the pull-off of the fibre in Gao's work is a result of crack propagation. In the flaw sensitive regime, Gao *et al.* obtained the pull-off stress by applying the Griffith energy balance criterion at the crack tip. The result is a linear relation between $\sigma_s$ and $\chi^{-1/2}$. In the flaw insensitive regime, Gao *et al.* also used equation (3.8). Similar analysis on different systems has been carried out by Persson (2003*a*) to characterize the flaw sensitive to flaw insensitive failure in the adhesion of small-sized bodies with other geometries.

### 3.2. Numerical results

Finite element simulations were carried out using Abaqus (Hibbit, Karlsson & Sorensen, Inc.) for the pull-off of an elastic fibre from a rigid substrate. The

fibre is assumed to be nearly incompressible with $\nu = 0.49$. The DB cohesive zone model is implemented for different values of $\chi$. Some details of the simulations are given in appendix C.

Figure 4 plots the normalized pull-off stress $\sigma_s/\sigma_0 = \Phi(\chi)$ versus $\chi$. The asymptotic behaviour of $\Phi(\chi)$ in the flaw sensitive regime, equation (3.6), is plotted on the same figure as a comparison. Although equation (3.6) is supposed to be valid for very large $\chi$, our finite element results show that it is an excellent approximation right up to the transition point, $\chi = \chi_T \approx 0.7$, where $\Phi(\chi)$ abruptly levels out. For $\chi \ll \chi_T$, the normalized pull-off stress is 1, as predicted by equation (3.8).

To summarize, the normalized pull-off stress for a nearly incompressible fibre is well approximated by

$$\sigma_s/\sigma_0 = \Phi(\chi) = \begin{cases} B\chi^{-\lambda} & \chi > \chi_T, \\ 1 & \chi \le \chi_T, \end{cases} \tag{3.11}$$

where $\lambda \approx 0.4$. The constant $B$ is determined using our finite element result, and it is 0.83.

It should be noted that for fibrils appearing in biological systems, the material does not need to be incompressible. However, there is no difficulty extending our analysis to that situation. Indeed, the asymptotic result (3.10) is expected to be true for all materials, and $\lambda$ varies with $\nu$ according to figure 7 (see appendix A). The constant $B$, which is expected to be of order one, for a particular Poisson's ratio $\nu$ can be obtained by carrying out finite element simulations.

## 4. STRENGTH OF A FIBRILLAR INTERFACE

Equations (1.5) and (3.11) allow us to address the question whether it is possible for the fibrillar structure in figure 1*b* to have a higher strength than the non-fibrillar structure in figure 1*a*. In the following, we assume that the large 'fibre' or the non-fibrillar interface in figure 1*a* is in the flaw sensitive regime where $\chi(A) \equiv \sigma_0^2 A/2\pi E^* W_{ad} > \chi_T$, and discuss two possible strength scenarios for the fibrillar interface shown in figure 1*b*.

*Case I*: $\chi(a) \equiv \sigma_0^2 a/2\pi E^* W_{ad} \le \chi_T$ (small fibrils)

In this case, the fibrils are in the flaw insensitive regime. Using equation (3.11), $\sigma_s(a)$ and $\sigma_s(A)$ can be evaluated. Substituting them into equation (1.5) gives

$$\omega > B[\chi(A)]^{-\lambda}. \tag{4.1}$$

Equation (4.1) implies that the strength of fibrillar structure in figure 1*b* is higher than the non-fibrillar one in figure 1*a* as long as

$$A > \frac{2\pi E^* W_{ad}}{\sigma_0^2}\left(\frac{B}{\omega}\right)^{1/\lambda}. \quad \text{(Case I)}. \tag{4.2}$$

*Case II*: $\chi(a) > \chi_T$

In this case, the fibrils are also in the flaw sensitive regime, and equation (1.5) becomes

$$A > a\omega^{-1/\lambda}. \quad \text{(Case II)}. \tag{4.3}$$

The scaling law (4.3) depends only on the geometry and is independent of material properties. This conclusion, however, is not exactly true, since when the fibrils are too close (i.e. large $\omega$); they tend to stick laterally to reduce surface energy, which prevents them from making good contact. This phenomenon has been studied by several investigators (Hui *et al.* 2002; Persson 2003*b*; Sitti & Fearing 2003; Glassmaker *et al.* 2004) using similar approaches but with different geometries. In this work, we use the result obtained by Glassmaker *et al.* (2004) since they consider both lateral and cross-sectional elastic deformations of the fibril during lateral sticking. It has been shown by Glassmaker *et al.* (2004) that to prevent sticking of two cylindrical fibrils of radius $a$, they have to be separated by at least a distance of $a\eta_{min}$, where

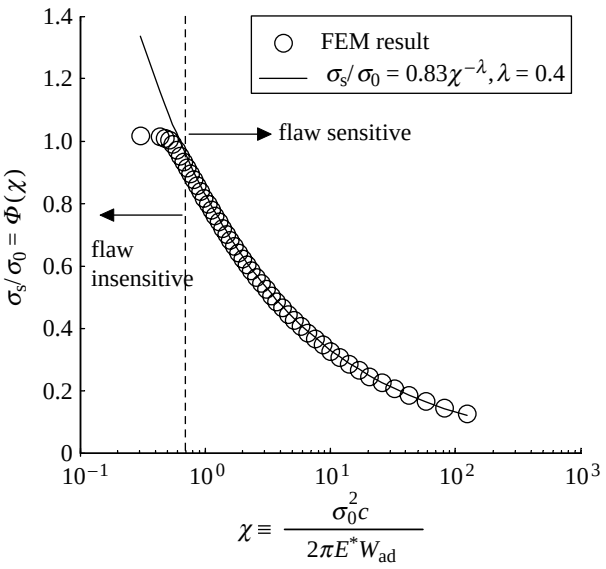


Figure 4. Dependence of pull-off stress on dimensionless parameter $\chi = \sigma_0^2 c/2\pi E^* W_{ad}$. Circles are finite element results. Solid line denotes asymptotic behaviour of $\Phi(\chi)$ for large $\chi$, given by equation (3.6).

$$\eta_{min} = \left(\frac{2^{11}\gamma_s}{\pi^4 E^* a}\right)^{1/6}\left(\frac{\gamma_s}{3Ea}\right)^{1/2}\left(\frac{h}{a}\right)^2, \tag{4.4}$$

$h$ is the height of the fibrils and $\gamma_s$ is the surface energy of the material of the fibrils. For cylindrical fibrils distributed uniformly on a square lattice with spacing $\eta a$,[3] the area fraction is

$$\omega = \frac{\pi}{(\eta+2)^2}. \tag{4.5}$$

Substituting equation (4.5) into equations (4.2) and (4.3) gives the conditions for a fibrillar interface in figure 1*b* to be stronger than a non-fibrillar one in figure 1*a*

$$A > \frac{2\pi E^* W_{ad}}{\sigma_0^2}\left[\frac{B(\eta+2)^2}{\pi}\right]^{1/\lambda} \quad \text{and} \quad \eta \ge \eta_{min}$$
$$\left(\text{Case I}: \ \frac{\sigma_0^2 a}{2\pi E^* W_{ad}} \le \chi_T\right), \tag{4.6}$$

[3]We have chosen a square lattice for simplicity; a hexagonal close packed configuration will give the largest $\omega$ for a given spacing.

Table 1. Examples of strength and toughness of a fibrillar interface in the flaw insensitive and flaw sensitive regimes for two types of materials.

| | soft materials, e.g. PDMS | | stiff materials, e.g. keratin | |
|---|---|---|---|---|
| $E$ (MPa) | 1 | | 2000 | |
| $\nu$ | 0.5 | | 0.5 | |
| $\gamma_s$ (mJ m$^{-2}$) | 50 | | 50 | |
| $W_{ad}$ (mJ m$^{-2}$) | 50 | | 50 | |
| $\sigma_0$ (MPa) | 0.1 | | 20 | |
| | flaw insensitive | flaw sensitive | flaw insensitive | flaw sensitive |
| $a$ (μm) | 10 | 100 | 1 | 10 |
| $\chi$ | 0.24 | 2.4 | 0.48 | 4.8 |
| $h=10a$ (μm) | 100 | 1000 | 10 | 100 |
| $\eta_{min}$ | 2.67 | 0.58 | 0.08 | 0.017 |
| $\omega_{max}$ | 0.14 | 0.47 | 0.73 | 0.77 |
| condition for fibrillar interface to be stronger at $\omega=\omega_{max}$ | $A>3.35$ mm | $A>0.65$ mm | $A>3$ μm | $A>19$ μm |
| | a common value of $A=4$ mm is used to calculate $F_s$ and $W_f$ below | | a common value of $A=20$ μm is used to calculate $F_s$ and $W_f$ below | |
| $\sigma_s$ (MPa) | 0.1 | 0.06 | 20 | 8.88 |
| $F_s$ (N) at $\omega=\omega_{max}$ | 0.72 | 1.39 | 0.02 | 0.01 |
| $W_f$ (J) at $\omega=\omega_{max}$ | $3.98\times10^{-6}$ | $4.21\times10^{-5}$ | $9.6\times10^{-10}$ | $1.96\times10^{-9}$ |

$$A > a\frac{(\eta+2)^{2/\lambda}}{\pi^{1/\lambda}} \quad \text{and} \quad \eta \geq \eta_{min}$$

$$\left(\text{Case II}: \frac{\sigma_0^2 a}{2\pi E^* W_{ad}} > \chi_T\right). \tag{4.7}$$

For a very soft incompressible material with van der Waals surface interactions, e.g. PDMS, $E\approx1$ MPa, $\nu\approx0.5$ and $\gamma_s\approx50$ mJ m$^{-2}$. Since it is unlikely for the intrinsic strength of the fibril/substrate interface to exceed the fibril modulus (Hui *et al.* 2003), we assume $\sigma_0\approx0.1$ MPa, $W_{ad}\approx50$ mJ m$^{-2}$, and the aspect ratio of the fibrils is $h/a=10$. Table 1 compares the strength of two geometries, one of which lies in the flaw insensitive regime, and the other lies in the flaw sensitive regime. The minimum spacing $\eta_{min}$ between the fibrils to avoid lateral collapse is calculated using equation (4.4). The corresponding maximum area fraction $\omega_{max}$ of fibrils is obtained from equation (4.5) by using $\eta=\eta_{min}$. Substituting $\eta=\eta_{min}$ into equations (4.6) and (4.7), we obtained the conditions, i.e. the ranges of $A$, for a fibrillar interface to be stronger than a non-fibrillar one, if the fibrillar interface has its maximum allowed area fraction. These are the most conservative conditions for $A$ because $A$ needs to be greater if $\omega<\omega_{max}$. Using equation (1.3) and a common value of $A$ that satisfies the above conditions, we calculated the strength $F_s$ of a fibrillar interface at $\omega=\omega_{max}$ in both the flaw insensitive and flaw sensitive regimes.

It can be seen from table 1 that although the single fibre pull-off stress $\sigma_s$ is higher in the flaw insensitive regime, the strength of the fibrillar interface in this regime may be lower than that in the flaw sensitive regime. This is because the strength is directly proportional to $\omega$, while the area fraction allowed in the flaw insensitive regime is much lower. Therefore, the compliance of the fibrils and hence lateral collapse impose a very large constraint on the strength. The same estimates can be carried out for a stiffer material. For example, the material found in gecko setae, keratin, has a modulus of about 2 GPa. Using the same $\gamma_s$, $W_{ad}$ and aspect ratio $h/a$, while assuming $\sigma_0\approx20$ MPa (Gao *et al.* 2005), the maximum area fraction is found to be about the same for the flaw insensitive and flaw sensitive regime (see table 1), and therefore for the same $A$, the strength is higher in the flaw insensitive regime. It can be seen from above analysis that there is an optimal range of fibril sizes in which higher strength can be obtained. For soft materials, this range lies in the flaw sensitive regime; while for stiff materials, it lies in the flaw insensitive regime. Note that in all cases, the strength of a fibrillar interface exceeds its non-fibrillar counterpart when $A$ is greater than the critical value specified in table 1.

## 5. TOUGHNESS OF A FIBRILLAR INTERFACE

To increase toughness, energy must be dissipated. Since the system is elastic, and the surface interaction is rate independent, one would expect the toughness $W_f$ for the structures shown in figure 1*a*,*b* to be $\pi A^2 W_{ad}$ and $\omega\pi A^2 W_{ad}$, respectively; so that the non-fibrillar interface should have a higher toughness. That this need not be the case was explored by Jagota & Bennison (2002), who pointed out that there is an analogy between the failure of a fibrillar interface and that of rubbery materials. Lake & Thomas (1967) noted that the fracture energies of rubbery solids are much higher than the energy required to sever carbon–carbon bonds. By assuming all the elastic energy stored between cross-links is lost whenever any bond between the two is severed, they established a scaling relation between molecular entanglements and the fracture energy. Furthermore, they demonstrated that their theory could explain their experimental data. Based on this idea, Jagota & Bennison (2002) proposed that, for sufficiently long and thin fibrils, the elastic strain energy stored in the fibrils is not recoverable at pull-off. By this argument, the total energy dissipated in a

fibrillar interface is

$$W_{\mathrm{f}} = \omega\pi A^2\left(\frac{\sigma_{\mathrm{s}}^2}{2E}h + W_{\mathrm{ad}}\right), \tag{5.1}$$

where $\sigma_{\mathrm{s}}$ is the pull-off stress determined by equation (3.11), and $h$ is the height of a fibril. Equation (5.1) implies that a fibrillar interface is tougher if $W_{\mathrm{f}} > \pi A^2 W_{\mathrm{ad}}$, i.e.

$$\frac{\sigma_{\mathrm{s}}^2}{2E}h > \frac{1-\omega}{\omega}W_{\mathrm{ad}}. \tag{5.2}$$

Since $\sigma_{\mathrm{s}}$ increases as the size of the fibrils decrease, equation (5.2) indicates that an interface consisting of thin and long fibrils, under the condition that no lateral collapse occurs, can have both higher strength and higher toughness than a non-fibrillar interface.

The toughness $W_{\mathrm{f}}$ at $\omega = \omega_{\max}$ is computed in table 1 using (5.1) for two types of material in both flaw insensitive and flaw sensitive regimes. In all the four cases, inequality (5.2) is satisfied, indicating the fibrillar interface is tougher. Similarly to the strength, the toughness in the flaw sensitive regime may be higher than that in the flaw insensitive regime due to the lateral collapse constraint. Note that in table 1, the toughness of the stiff materials in the flaw sensitive regime is still greater even though the area fraction in this regime is about the same as that in the flaw insensitive regime. The reason of this result is that we used the same aspect ratio $h/a$ in the calculations so that $h$ in the flaw sensitive regime is much larger. Since in equation (5.1) the elastic energy stored in the fibrils is directly proportional to $h$, $W_{\mathrm{f}}$ is significantly increased.

## 6. DISCUSSIONS AND CONCLUSION

It is interesting to compare our analysis with the contact mechanics theories of Johnson–Kendall–Roberts (JKR 1971) and Maugis (1992). These theories have been used by many authors (Arzt *et al.* 2003; Sitti & Fearing 2003; Peressadko & Gorb 2004) to determine the scaling rule governing the adhesion of geckos. Instead of having flat contact, these theories allow that one or both of the surfaces in contact are spherical, e.g. each fibril ends with a spherical tip of radius $R$. Generally it is implicitly assumed that $R$ is of the same order as the fibre radius $a$ as shown in figure 5*b*.

The JKR theory is an extension of the Hertz theory of contact, in that it accounts for the adhesion of spherical lenses by including the effect of attractive surface forces that act when the bodies are in contact. These surfaces forces are modified by adding a tensile stress distribution to the usual compressive Hertz pressure that exists in the contact region. Because it is only within the contact region that the stresses are modified, the JKR theory ignores any surface forces that act outside the contact region, and, therefore, may not be applicable when the contact region is small. A limitation of the JKR theory is that tensile stresses are unbounded at the edge of the contact region. In reality, however, cohesive forces will act outside the contact region, and they will serve to place a limit on the maximum stress that is reached. Because of this, attempts to better model adhesion contact have been made by accounting for surface forces that act outside the contact edge. Derjaguin–Muller–Toporov (DMT 1975) proposed a theory that takes these forces into account, but assumes that they do not change the shape of the deformed surfaces from the Hertzian profile. This approximation leads to adhesion (tensile) stresses that are finite outside the contact zone but are zero inside. A unifying model of elastic contact was proposed by Maugis (1992), who used the DB model to represent the surface forces outside the contact zone, and found that the transition from JKR to DMT theory can be characterized using a dimensionless Tabor parameter

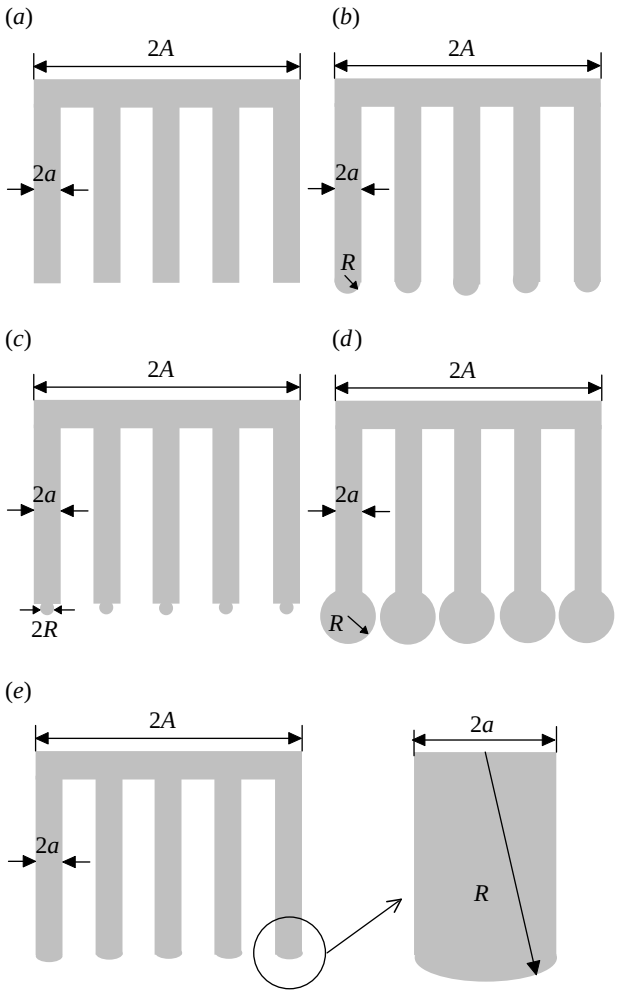


Figure 5. Comparison between different fibrillar structures. (*a*) Flat end fibrils with radius $a$. (*b*) Fibrils with a spherical tip of radius $R \approx a$. (*c*) Fibrils with a spherical tip of radius $R \ll a$. (*d*) Fibrils with a spherical tip of radius $R \gg a$. (*e*) Fibrils with a shallow spherical tip.

$$\lambda_{\mathrm{Maugis}} \equiv \frac{2\sigma_0}{[16\pi W_{\mathrm{ad}}(E^*)^2/9R]^{1/3}}. \tag{6.1}$$

Analogous to the adhesion of flat interfaces considered in this paper, JKR theory corresponds to the flaw sensitive regime and is valid when $\lambda_{\mathrm{Maugis}} \gg 1$. On the other hand, DMT theory corresponds to the flaw insensitive regime and is applicable when $\lambda_{\mathrm{Maugis}} \ll 1$. The force needed to pull off a single fibre with tip radius $R$ is

predicted respectively by JKR and DMT theories as

$$f_s^{JKR} = 3\pi R W_{ad}/2, \tag{6.2}$$

$$f_s^{DMT} = 2\pi R W_{ad}. \tag{6.3}$$

Assuming the fibre radius $a \approx R$, the average pull-off stress for the two theories are

$$\sigma_s^{JKR} \approx f_s^{JKR}/\pi R^2 \approx 3\,W_{ad}/2R, \tag{6.4}$$

$$\sigma_s^{DMT} \approx f_s^{DMT}/\pi R^2 \approx 2\,W_{ad}/R. \tag{6.5}$$

Equations (6.4) and (6.5) imply that the pull-off stress increases as $R$ decreases, consistent with our results, although the dependence of $\sigma_s$ on $R$ is different from equation (3.11). Unlike the case of flat fibrils, the difference in the single fibre pull-off stress between the flaw sensitive and flaw insensitive regime is small, i.e. $(\sigma_s^{DMT} - \sigma_s^{JKR})/\sigma_s^{DMT} = 1/4$. Furthermore, neither theory gives an upper bound for the pull-off stress. Indeed, $\sigma_s^{JKR} \to \infty$, $\sigma_s^{DMT} \to \infty$ as $R \to 0$. In this limit, the fibre can never be pulled off! This inconsistency was also noted by Gao *et al.* (2005).

The above argument, however, is misleading because the application of JKR and DMT theories is subject to several restrictions. Specifically, in all three theories (JKR, DMT and Maugis), the lenses in contact are modelled as half spaces, and the region outside the contact zone is treated as a semi-infinite crack. This approximation is valid only if the size of the contact region is much smaller than the radius of the lenses. This condition for the JKR theory, if we use the contact radius at pull-off $a_{JKR} \approx (W_{ad}R^2/E^*)^{1/3}$, translates to

$$R \gg W_{ad}/E^* \quad \text{(JKR)}. \tag{6.6}$$

For the DMT theory, since the contact profile is locally parabolic, the interfacial opening at the contact edge is $a_{DMT}^2/2R$, where $a_{DMT}$ is the contact radius in the DMT theory. At pull off, the opening at the contact edge reaches $\delta_c$. Therefore, the condition $a_{DMT} \ll R$ is $\sqrt{2R\delta_c} \ll R$ or

$$R \gg \delta_c \quad \text{(DMT)}, \tag{6.7}$$

where we have neglected a numerical factor of order one. Equations (6.6) and (6.7) impose constraints on the radius of curvature $R$, so that the limit of $R \to 0$ is not meaningful. A further restriction is Maugis' transition condition: $\lambda_{Maugis} \gg 1$ in JKR theory, and $\lambda_{Maugis} \ll 1$ in DMT theory, where $\lambda_{Maugis}$ is defined by equation (6.1). This condition results in

$$R \gg \frac{2\pi W_{ad}(E^*)^2}{9\sigma_0^3} \quad \text{(JKR)}, \tag{6.8}$$

$$R \ll \frac{2\pi W_{ad}(E^*)^2}{9\sigma_0^3} \quad \text{(DMT)}. \tag{6.9}$$

For a soft incompressible material and an interface dominated by van der Waals interaction, $E \approx 1$ MPa, $\nu \approx 0.5$ and $W_{ad} \approx 50$ mJ m$^{-2}$. Let $\sigma_0 = E/10 = 0.1$ MPa, the right-hand side of equations (6.6) and (6.8) are 38 and 62 μm, respectively. Thus, JKR theory is applicable if $R \gg 62$ μm. Using $\delta_c = W_{ad}/\sigma_0$, equations (6.7) and (6.9) predict that DMT theory is applicable provided that $R$ satisfies the inequality $0.5\ \mu m \ll R \ll 62\ \mu m$.

For a stiffer material such as keratin, $E \approx 2$ GPa; assuming $\sigma_0 = 20$ MPa (Gao *et al.* 2005), the applicability of JKR theory require $R \gg 31$ μm, while DMT theory is valid for $2.5\ nm \ll R \ll 31\ \mu m$. In this case, it is likely that DMT theory would be more appropriate, since the radius of fibrils in biological systems is typical in the 1 μm range. However, as can be seen from equations (6.8) and (6.9), the usage of the two theories strongly depends on the intrinsic strength $\sigma_0$, while a good estimate of the intrinsic strength of keratin is not available from existing experimental data. For example, if we use $\sigma_0 = 100$ MPa instead, then JKR theory is valid when $R \gg 0.25$ μm, and DMT theory is valid when $0.5\ nm \ll R \ll 0.25\ \mu m$. In this situation, the use of JKR theory would be justified.

Physically, one expects that the strength of the flat-ended fibrils in figure 5*a* must be stronger the spherical-ended fibrils in figure 5*b*. For simplicity, we compare the flaw insensitive regimes of both structures, where they obtain their highest strength. The flaw insensitive regime of figure 5*a* corresponds to uniform stress distribution $\sigma_0$ on the interface. Therefore the strength is

$$F_s^{(a)} = N f_s^{(a)} = \omega\pi A^2\sigma_0, \tag{6.10}$$

where $N$ is the total number of fibrils, and $\omega = Na^2/A^2$ is the area fraction. The flaw insensitive regime of figure 5*b* corresponds to the DMT limit, and the strength is

$$F_s^{(b)} = N f_s^{(b)} \approx \frac{\omega A^2}{R^2} 2\pi R W_{ad} = \omega\pi A^2\sigma_0\left(\frac{2\delta_c}{R}\right), \tag{6.11}$$

where $W_{ad} = \sigma_0\delta_c$ and $R \approx a$ have been used. According to equation (6.7), $\delta_c/R \ll 1$. Therefore, equation (6.10) is much larger than equation (6.11), indicating a flat-ended structure has better adhesion than a spherical-ended one with the same area fraction.

As shown by Persson (2003*a*,*b*), plate-like structures found in geckos serve to improve adhesive contact on rough surfaces. However, since we are not only interested in geckos but also in fibrillar structures one can make with current technology, it is worthwhile to compare fibrillar interfaces with different tip structures, as shown in figure 5*c*–*e*. The strength of the fibrillar interface in figure 5*c*, where $R \ll a$, is

$$F_s^{(c)} = N f_s^{(c)} = \frac{\omega A^2}{a^2} 2\pi R W_{ad} = \omega\pi A^2\sigma_0\left(\frac{2\delta_c}{R}\right)\left(\frac{R}{a}\right)^2. \tag{6.12}$$

Since $\delta_c/R \ll 1$ and $R/a \ll 1$, the structure in figure 5*a* is stronger than the one shown in figure 5*c*. However, the strength of the structure shown in figure 5*d*, where $R \gg a$, can be higher than the strength of the flat-ended structure. Specifically

$$F_s^{(d)} = N f_s^{(d)} = \frac{\omega A^2}{a^2} 2\pi R W_{ad} = \omega\pi A^2\sigma_0\left(\frac{2\delta_c}{R}\right)\left(\frac{R}{a}\right)^2. \tag{6.13}$$

Since $R/a \gg 1$, $F_s^{(d)}$ can be greater than $F_s^{(a)}$. This reasoning is flawed since we have implicitly assumed that $\omega$ is the same for both structures, whereas in

reality, $\omega$ for the structure in figure 5*d* is much less. This is due to the fact that the lateral collapse condition (4.4) must be modified because the spheres can stick to each other before the sides make contact. More significantly, because of the spherical tip, the number of fibrils allowed on the interface cannot exceed $A^2/R^2$, i.e.

$$F_{\mathrm{s}}^{(d)} = N f_{\mathrm{s}}^{(d)} < \frac{A^2}{R^2} 2\pi R W_{\mathrm{ad}} = \omega \pi A^2 \sigma_0 \left(\frac{2\delta_{\mathrm{c}}}{\omega R}\right), \quad (6.14)$$

where $\omega$ denotes the area fraction of the structure in figure 5*a*. Since in general $\delta_{\mathrm{c}}/R \ll \omega$, equation (6.14) is much smaller than $\omega\pi A^2\sigma_0$, the strength of the structure in figure 5*a*.

There has been some confusion in current literature regarding the strength of a spherically tipped fibrillar interface. For example, in a recent work, Spolenak *et al.* (2005) have explored the influence of contact end shape. While providing several enlightening results on the scaling of the strength for the various shapes they consider, our work shows that these results are not universally applicable. Specifically, they consider a scenario in which a fibre with a spherical end of radius of curvature $R$ subdivides into $N$ fibrils with tips having the same radius of curvature and show that the strength of such an interface (figure 5*e*) can be higher than a fibrillar interface with flat tips (figure 5*a*). In this case, usage of the JKR theory will predict

$$F_{\mathrm{s}}^{(e)} = N f_{\mathrm{s}}^{(e)} = \frac{\omega A^2}{a^2} \frac{3\pi R W_{\mathrm{ad}}}{2} \quad (\mathrm{JKR}), \quad (6.15)$$

where $F_{\mathrm{s}}^{(e)}$ is the strength of the fibril bundle in figure 5*e*. Comparing equation (6.15) with the strength of figure 5*a* in the flaw sensitive regime, i.e.

$$F_{\mathrm{s}}^{(a)} = \omega \pi A^2 \left[0.83\sigma_0 \left(\frac{\sigma_0^2 a}{2\pi E^* W_{\mathrm{ad}}}\right)^{-0.4}\right] \quad (\text{flaw sensitive}), \quad (6.16)$$

we found

$$F_{\mathrm{s}}^{(e)} = F_{\mathrm{s}}^{(a)} \frac{3}{1.66} \left[\frac{W_{\mathrm{ad}}^3 R^5}{(2\pi E^*)^2 \sigma_0 a^8}\right]^{1/5} \quad (\mathrm{JKR}). \quad (6.17)$$

Since $R \gg a$, it seems that equation (6.15) can be much greater than equation (6.16). This argument, however, is flawed, since the geometric constraints for the use of the JKR theory have not been taken into account. Specifically in this case, the contact area for each fibril can never exceed the size of the fibril. Indeed, for the half space assumption in the JKR theory to be valid, the contact radius $a_{\mathrm{JKR}} \approx (W_{\mathrm{ad}} R^2/E^*)^{1/3} \ll a$. Substituting this inequality into (6.17) results in

$$F_{\mathrm{s}}^{(e)} \ll F_{\mathrm{s}}^{(a)} \left[\frac{W_{\mathrm{ad}} (E^*)^2}{\sigma_0^3 R}\right]^{1/15} \quad (\mathrm{JKR}). \quad (6.18)$$

Maugis transition condition (6.8) implies that JKR theory is valid as long as $W_{\mathrm{ad}}(E^*)^2/\sigma_0^3 R \ll 1$, therefore equation (6.18) indicates the strength of the fibril bundle in figure 5*e* can never exceed that of figure 5*a*. Indeed, if equation (6.15) were larger than equation (6.16), then the contact radius at pull-off has to be much greater than the fibril radius for the interface, which is impossible. An equivalent argument is that for a given tip radius $R$, the numbers of fibrils allowed for using the JKR theory in figure 5*e* have an upper bound, i.e. the following condition must be satisfied

$$N = \frac{\omega A^2}{a^2} \ll \omega A^2 \left(\frac{E^*}{W_{\mathrm{ad}} R^2}\right)^{2/3}. \quad (6.19)$$

Likewise, it can be easily shown that the strength of the fibril bundle in figure 5*e* is still lower than that of figure 5*a*, if one assumes that adhesion is in the DMT regime. That is,

$$F_{\mathrm{s}}^{(e)} = \frac{\omega A^2}{a^2} 2\pi R W_{\mathrm{ad}} \ (\mathrm{DMT}). \quad (6.20)$$

Comparing equation (6.20) with the strength of figure 5*a* in the flaw insensitive regime, equation (6.10), results in

$$F_{\mathrm{s}}^{(e)} = F_{\mathrm{s}}^{(a)} \frac{2R\delta_{\mathrm{c}}}{a^2} = F_{\mathrm{s}}^{(a)} \left(\frac{a_{\mathrm{DMT}}}{a}\right)^2 \ll F_{\mathrm{s}}^{(a)} \ (\mathrm{DMT}), \quad (6.21)$$

where the last statement is true because $a_{\mathrm{DMT}}/a \ll 1$. Note that $a_{\mathrm{DMT}}$ must be less than $a_{\mathrm{JKR}}$ at the same applied load, since the geometry is not changed by adhesive surface forces in the DMT theory. Physically, a flat-ended fibrillar interface is better than a spherically ended one because the average stress on each spherically ended fibril can never reach the interfacial strength $\sigma_0$, which is the average stress on each flat-ended fibril in the flaw insensitive limit.

Even with the assumption of perfect uniform contact, for compliant fibrils, lateral collapse can be detrimental to the adhesion of a fibrillar interface. Of course, perfect uniform contacts do not occur in natural systems. This means that the strength and toughness derived here are theoretical upper bounds. Indeed, recent work by Persson & Tosatti (2001), Persson & Gorb (2003) and Hui *et al.* (in press) have demonstrated that rough surface can reduce both the strength and the effective work of adhesion in a significant way. For example, when a rough surface is in contact with a fibrillar structure, some fibrils are under compression whereas others are in tension, as illustrated in figure 6. This means that fibrils will not be pulled off uniformly, resulting in much lower strength and toughness. This is the reason why plate-like spatula structures are found in geckos to lower the contact resistance. Also, the fibrils can buckle to increase the compliance of the system. Indeed, if the fibrils in figure 6 have spherical tips, then the mean pull-off force decreases with increasing roughness height standard deviation: the relationship is linear for small height variance, and the pull off force trails off to zero for very rough surfaces (Hui *et al.* in press). On the other hand, the work of separation is shown to be unaffected by small roughness height standard deviation, although it decreases toward zero for rougher surfaces. The effects of roughness may be offset by increasing fibrillar compliance; for small roughness height standard deviation, Hui *et al.* (in press) showed that the reduction in the pull off force is inversely proportional to the normalized compliance. Also, the work of separation increases

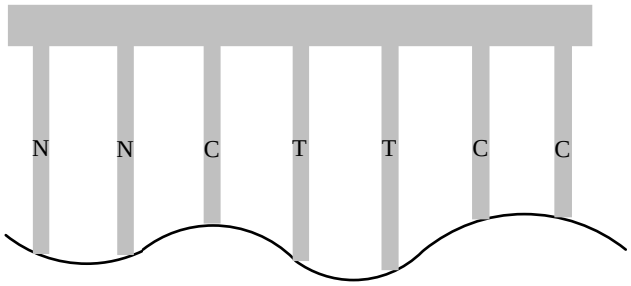


Figure 6. Illustration of a fibrillar structure on a rough surface. Some fibrils are in tension, marked with 'T', some are in compression, marked with 'C', and some are neutral, marked with 'N'. This figure is for demonstrating the effect of roughness. In the analysis by Hui *et al.* (in press), the fibrils are considered to be springs, and the compliance of the springs can be computed based on beam bending.

linearly with the compliance when the compliance is large compared to the roughness height variance.

To conclude, our analysis shows that it is possible for a fibrillar interface to be both stronger and tougher than a flat one even in a purely elastic system, provided that the conditions (4.6), (4.7) and (5.2) are satisfied. However, lateral collapse puts a significant constraint on the strength and toughness of a fibrillar interface by limiting the area fraction of the fibrils. In fact, we have examples for which the strength and toughness of a fibrillar interface are both lower in the flaw insensitive regime than in the flaw sensitive regime. In actual physical systems, the roughness of the surface can also be detrimental to the strength and toughness of a fibrillar interface.

We acknowledge Prof. Anand Jagota of Lehigh University, who has had many discussions with us and also allowed us to use his finite element program.

## APPENDIX A. DETERMINATION OF STRESS SINGULARITY $\lambda$ AT CORNER OF THE ELASTIC FIBRE

The asymptotic behaviour of the elastic solution near the corner of the fibre can be examined using the method proposed by Bogy & Wang (1971) and Dempsey & Sinclair (1981). Assume the stresses near the corner are proportional to $\rho^{-\lambda}$, where $\rho$ is the distance from the corner, shown in figure 3*b*, and $\lambda$ is the singularity. Using a complex variable analysis (Bogy & Wang 1971) and boundary conditions, the equation governing the singularity is found to be

$$4(1-\lambda)^2-2\kappa\cos\pi(1-\lambda)-(\kappa^2+1)=0, \qquad \text{(A 1)}$$

where $\kappa\equiv 3-4\nu$, and $\nu$ is the Poisson's ratio. We seek solution for $0<\lambda<1$. Figure 7 shows the numerical result for the relation between $\lambda$ and Poisson's ratio $\nu$. For each $\nu$, there is a unique solution between 0 and 1. In particular, for an incompressible material, $\nu=0.5$, $\kappa=1$ and $\lambda\approx 0.4$.

It should be noted that as shown by Dempsey *et al.* (Dempsey & Sinclair 1981), singular stress field of the form $\rho^{-\lambda}\ln\rho$ can exist for certain special material combinations. We have not considered these special cases.

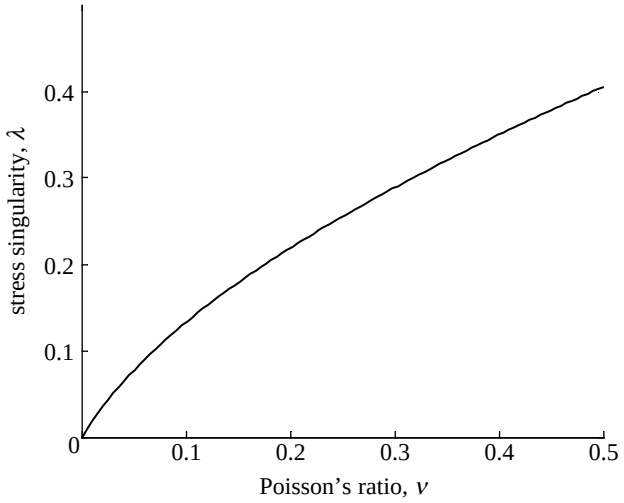


Figure 7. Stress singularity at the corner of the elastic fibre versus Poisson's ratio of the material.

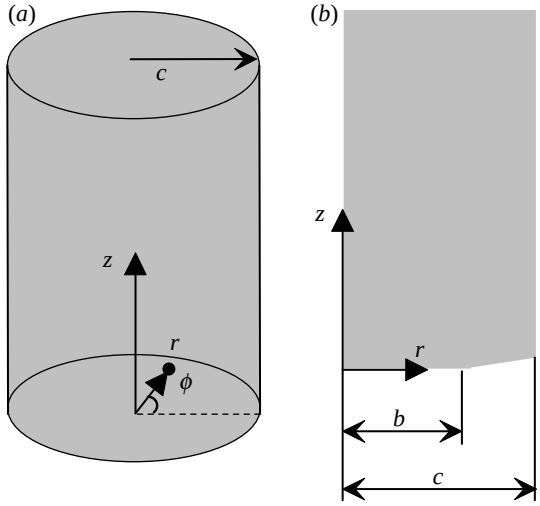


Figure 8. (*a*) Cylindrical coordinate system of the fibre. (*b*) Cohesive zone generated in the region $b\leq r\leq c$.

## APPENDIX B. DEPENDENCE OF THE NORMALIZED PULL-OFF STRESS $\sigma_s/\sigma_0$ ON A SINGLE DIMENSIONLESS PARAMETER $\chi\equiv\sigma_0^2 c/2\pi E^* W_{ad}$

Consider the pull-off of a cylindrical elastic fibre with radius $c$ on a rigid substrate under a far field loading stress $\sigma$. The elastic fibre has Young's modulus $E$ and Poisson's ratio $\nu$. The DB cohesive zone model is introduced on the interface between the fibre and the substrate, with the intrinsic strength $\sigma_0$ and the critical opening $\delta_c$. The coordinate system used in the formulation is shown in figure 8. Let $u_i$, $\varepsilon_{ij}$ and $\sigma_{ij}$ denote the displacement, strain and stress components, respectively.

Because of axis-symmetry, the non-zero displacement components for this problem are $u_r=u_r(r,z)$ and $u_z=u_z(r,z)$. Introduce the following normalization:

$$\bar{r}\equiv r/c,\quad \bar{z}\equiv z/c,\quad \bar{u}_i\equiv Gu_i/\sigma c,$$
$$\bar{\sigma}_{ij}\equiv\sigma_{ij}/\sigma_0,\quad \bar{e}\equiv(\bar{r}\,\bar{u}_r)_{,\bar{r}}/\bar{r}+\bar{u}_{z,\bar{z}}, \qquad \text{(B 1)}$$

where $G=E/2(1+\nu)$ is the shear modulus. $\bar{u}_{z,\bar{z}}$ denotes the partial derivative of $\bar{u}_z$ with respect to $\bar{z}$ and so on. The equilibrium equations in terms of the normalized quantities are

$$\frac{1-\nu}{1-2\nu}\frac{\partial \bar{e}}{\partial \bar{r}}+\frac{\partial}{2\partial \bar{z}}\left(\frac{\partial \bar{u}_r}{\partial \bar{z}}-\frac{\partial \bar{u}_z}{\partial \bar{r}}\right)=0, \tag{B 2a}$$

$$\frac{1-\nu}{1-2\nu}\frac{\partial \bar{e}}{\partial \bar{z}}+\frac{1}{2\bar{r}}\frac{\partial}{\partial \bar{r}}\left[\bar{r}\left(\frac{\partial \bar{u}_r}{\partial \bar{z}}-\frac{\partial \bar{u}_z}{\partial \bar{r}}\right)\right]=0, \tag{B 2b}$$

which depend only on the Poisson's ratio. Under the far field loading $\sigma$, a cohesive zone is generated in the annulus $b\leq r\leq c$. The boundary conditions before pull-off are

$$\bar{\sigma}_{rr}(\bar{r}=1)=\frac{2\sigma}{\sigma_0}\left(\frac{\partial \bar{u}_r}{\partial \bar{r}}+\frac{\nu \bar{e}}{1-2\nu}\right)|_{\bar{r}=1}=0, \tag{B 3a}$$

$$\bar{\sigma}_{rz}(\bar{r}=1)=\frac{2\sigma}{\sigma_0}\left(\frac{\partial \bar{u}_r}{\partial \bar{z}}+\frac{\partial \bar{u}_z}{\partial \bar{r}}\right)|_{\bar{r}=1}=0, \tag{B 3b}$$

$$\bar{u}_r(\bar{r}<1,\bar{z}=0)=0, \tag{B 3c}$$

$$\bar{u}_z(\bar{r}<b/c,\bar{z}=0)=0, \tag{B 3d}$$

$$\bar{\sigma}_{zz}(b/c<\bar{r}<1,\bar{z}=0)=\frac{2\sigma}{\sigma_0}\left(\frac{\partial \bar{u}_z}{\partial \bar{z}}+\frac{\nu \bar{e}}{1-2\nu}\right)|_{b/c<\bar{r}<1,\bar{z}=0}=1, \tag{B 3e}$$

$$\bar{\sigma}_{zz}(\bar{r}<1,\bar{z}\to\infty)=\frac{2\sigma}{\sigma_0}\left(\frac{\partial \bar{u}_z}{\partial \bar{z}}+\frac{\nu \bar{e}}{1-2\nu}\right)\Big|_{\bar{r}<1,\bar{z}\to\infty}=\frac{\sigma}{\sigma_0}. \tag{B 3f}$$

(B 3*a*) and (B 3*b*) are traction free conditions on outer surface, (B 3*c*) is full friction condition on the interface, (B 3*d*) is the contact condition, (B 3*e*) is the interfacial cohesive zone model, and (B 3*f*) is the far field loading condition. Note that $b$ is an unknown of the problem, and is part of the solution. From equilibrium equations (B 2*a*) and (B 2*b*) and boundary conditions (B 3*a–f*), it can be seen that, for a given Poisson's ratio $\nu$, the normalized displacements and stresses depend only one dimensionless parameter $\sigma/\sigma_0$.

Pull-off occurs when the displacement $u_z$ at the edge of the fibre $r=c$, $z=0$ reaches $\delta_c$, the critical opening in the DB model. Our analysis implies that at pull-off

$$\bar{u}_z(\bar{r}=1,\bar{z}=0)=Q\left(\frac{\sigma_s}{\sigma_0}\right)=\frac{G\delta_c}{\sigma_s c}=\frac{GW_{ad}}{\sigma_s\sigma_0 c}, \tag{B 4}$$

where $Q$ is a dimensionless function determined by finite element simulations. Thus, the pull-off stress is determined by the solution of the equation (B 4). Given the Poisson's ratio $\nu$, it has the form

$$\frac{\sigma_s}{\sigma_0}=\Phi(\chi), \tag{B 5}$$

where $\chi\equiv\sigma_0^2 c/2\pi E^* W_{ad}$. Finite element simulations are carried out to determine the function $\Phi(\chi)$ in equation (B 5).

## APPENDIX C. ABAQUS IMPLEMENTATION DETAILS

Since the normalized pull-off stress depends only on $\chi\equiv\sigma_0^2 c(1-\nu^2)/2\pi E W_{ad}$, we fix $\sigma_0$, $c$, $E$ and $\nu$ while varying $W_{ad}$ by varying $\delta_c$ in our simulations. In ABAQUS, four-node bilinear axisymmetric solid elements are used to mesh the elastic fibre with radius of 1 μm and height of 10 μm. The elastic fibre has Young's modulus 2 MPa and Poisson's ratio 0.49. A rigid plane is created under the fibre and the interface is assigned to have full friction by constraining the nodal displacement in the radial direction. DB cohesive (users) elements are defined on the interface with fixed intrinsic strength $\sigma_0=0.1$ MPa. The critical opening $\delta_c$ was varied in the simulations from 0.05 to 20 nm. For each $\delta_c$, a sufficiently large displacement is applied on the top of the fibre through incremental steps. A static stress analysis is carried out to obtain pull-off. The stress in the fibre far away from the interface is uniform and is $\sigma_s$ when pull-off occurs. $\sigma_s/\sigma_0$ versus $\chi=\sigma_0^2 c/2\pi E^* W_{ad}$ is plotted in figure 4.

## REFERENCES


Arzt, E., Gorb, S. & Spolenak, R. 2003 From micro to nano contacts in biological attachment devices. *Proc. Natl Acad. Sci. USA* **100**, 10 603–10 606. (doi:10.1073/pnas.1534701100.)

Autumn, K., Yiching, A., Liang, S., Hsieh, T., Zesch, W., Chan, W. P., Kenny, T. W., Fearing, R. & Full, R. J. 2000 Adhesive force of a single gecko foot-hair. *Nature* **405**, 681–685. (doi:10.1038/35015073.)

Barenblatt, G. I. 1962 Mathematical theory of equilibrium cracks in brittle fracture. *Adv. Appl. Mech.* **7**, 55–129.

Bogy, D. B. & Wang, K. C. 1971 Stress singularities at interface corners in bonded dissimilar isotropic elastic materials. *Int. J. Solids Struct.* **7**, 993–1005. (doi:10.1016/0020-7683(71)90077-1.)

Campolo, D., Jones, S. D. & Fearing, R. S. 2003 Fabrication of gecko foot-hair like nano structures and adhesion to random rough surfaces. *Nanotech., IEEE-Nano 2003 Third IEEE Conf.* **2**, 856–859. (doi:10.1109/NANO.2003.1230945.)

Dempsey, J. P. & Sinclair, G. B. 1981 On the singular behavior at the vertex of a bi-material wedge. *J. Elasticity* **11**, 317–327.

Derjaguin, B. V., Muller, V. M. & Toporov, Y. P. 1975 Effect of contact deformations on the adhesion of particles. *J. Colloid Interface Sci.* **53**, 314–326. (doi:10.1016/0021-9797(75)90018-1.)

Dugdale, D. S. 1960 Yielding of steel sheets containing slits. *J. Mech. Phys. Solids* **8**, 100–104. (doi:10.1016/0022-5096(60)90013-2.)

Gao, H., Wang, X., Yao, H., Gorb, S. & Arzt, E. 2005 Mechanics of hierarchical adhesion structures of geckos. *Mech. Mater.* **37**, 275–285. (doi:10.1016/j.mechmat.2004.03.008.)

Geim, A. K., Dubonos, S. V., Grigorieva, I. V., Novoselov, K. S., Zhukov, A. A. & Shapoval, S. Y. 2003 Microfabricated adhesive mimicking gecko foot-hair. *Nat. Mater.* **2**, 461–463. (doi:10.1038/nmat917.)

Glassmaker, N. J., Jagota, A., Hui, C. Y. & Kim, J. 2004 Design of biomimetic fibrillar interface. 1. Making contact. *J. R. Soc. Interface* **1**, 23–33. (doi:10.1098/rsif.2004.0004.)

Hui, C. Y., Jagota, A., Lin, Y. Y. & Kramer, E. J. 2002 Constraints on microcontact printing imposed by stamp deformation. *Langmuir* **18**, 1394–1407. (doi:10.1021/la0113567.)

Hui, C. Y., Jagota, A., Bennison, S. J. & Londono, J. D. 2003 Crack blunting and the strength of soft elastic materials. *Proc. R. Soc. A* **459**, 1489–1516. (doi:10.1098/rspa.2002.1057.)

Hui, C. Y., Glassmaker, N. J., Tang, T. & Jagota, A. 2004 Design of biomimetic fibrillar interface. 2. Mechanics of enhanced adhesion. *J. R. Soc. Interface* **1**, 35–48. (doi:10.1098/rsif.2004.0005.)

Hui, C. Y., Glassmaker, N. J. & Jagota, A. In press. How compliance compensates for surface roughness in fibrillar adhesion. *J. Adhesion*.

Jagota, A. & Bennison, S. J. 2002 Mechanics of adhesion through a fibrillar microstructure. *Integr. Comp. Biol.* **42**, 1140–1145.

Johnson, K. L., Kendall, K. & Roberts, A. D. 1971 Surface energy and the contact of elastic solids. *Proc. R. Soc. A* **324**, 301–313.

Lake, G. J. & Thomas, A. G. 1967 The strength of highly elastic materials. *Proc. R. Soc. A* **300**, 108–115.

Maugis, D. 1992 Adhesion of spheres: the JKR–DMT transition using a Dugdale model. *J. Colloid Interface Sci.* **150**, 243–269. (doi:10.1016/0021-9797(92)90285-T.)

Peressadko, A. & Gorb, S. N. 2004 When less is more: experimental evidence for tenacity enhancement by division of contact area. *J. Adhesion* **80**, 247–261. (doi:10.1080/00218460490430199.)

Persson, B. N. J. 2003*a* Nanoadhesion. *Wear* **254**, 832–834. (doi:10.1016/S0043-1648(03)00233-3.)

Persson, B. N. J. 2003*b* On the mechanism of adhesion in biological systems. *J. Chem. Phys.* **118**, 7614–7621. (doi:10.1063/1.1562192.)

Persson, B. N. J. & Gorb, S. 2003 The effect of surface roughness on the adhesion of elastic plates with application to biological systems. *J. Chem. Phys.* **119**, 11 437–11 444. (doi:10.1063/1.1621854.)

Persson, B. N. J. & Tosatti, E. 2001 The effect of surface roughness on the adhesion of elastic solids. *J. Chem. Phys.* **115**, 5597–5610. (doi:10.1063/1.1398300.)

Rischick, D. J., Austin, C. C., Petren, K., Fisher, R. N., Losos, J. B. & Ellers, O. 1996 A comparative analysis of clinging ability among pad-bearing lizards. *Biol. J. Linn. Soc.* **59**, 21–35. (doi:10.1006/bijl.1996.0052.)

Rose, J. H., Ferrante, J. & Smith, J. R. 1981 Universal binding energy curves for metals and bimetallic interfaces. *Phys. Rev. Lett.* **47**, 675–678. (doi:10.1103/PhysRevLett.47.675.)

Scherge, M. & Gorb, S. N. 2001 *Biological micro and nanotribology: nature's solutions*. Berlin: Springer.

Sitti, M. & Fearing, R. S. 2003 Synthetic gecko foot-hair micro/nano-structures as dry adhesives. *J. Adhes. Sci. Tech.* **17**, 1055–1073. (doi:10.1163/156856103322113788.)

Spolenak, R., Gorb, S., Gao, H. & Arzt, E. 2005 Effect of contact shape on the scaling of biological attachments. *Proc. R. Soc. A* **461**, 305–319. (doi:10.1098/rspa.2004.1326.)

Xu, X. & Needleman, A. 1994 Numerical simulations of fast crack growth in brittle solids. *J. Mech. Phys. Solids* **42**, 1397–1434. (doi:10.1016/0022-5096(94)90003-5.)